Increasing impacts of summer extreme precipitation and heatwaves in eastern China

Yulong Yao[1,2] · Wei Zhang[3,4] · Ben Kirtman[5]

Abstract

Extreme precipitation events (EPEs) and heatwaves (HWs) can trigger floods, droughts, and other natural disasters, resulting in severe socioeconomic losses in eastern China. However, the accurate links between EPEs and HWs and future changes in these extremes are not fully resolved, which potentially impedes disaster warning and preparedness efforts. This study examines historical and future changes in summer EPEs and HWs in eastern China based on observations and model outputs from the Coupled Model Intercomparison Project Phase 6. The results show that EPEs and HWs in eastern China have increased in the past four decades and are projected to rise in the future. According to multi-model projections, the Yangtze River Basin, along with areas to its south, are expected to experience an increase in compound disasters due to HWs and EPEs. High values of the multi-year mean total population exposure to EPEs and HWs are observed in the North China Plain, Yangtze River Delta, Sichuan Basin, and southeast coast. The total population exposure to EPEs shows a decreasing trend under Shared Socioeconomic Pathway (SSP) 245 and SSP585 scenarios during 2021–2100, consistent with future population decline. However, the annual total population exposure to HWs will increase, reaching nearly 3.0 billion and 5.0 billion by the end of the century under the SSP245 and SSP585 scenarios, respectively. Within the context of global warming, the relationship between the mean-state of precipitation and maximum temperature as well as the relationship between extreme precipitation and heatwaves shift from negative correlation in the historical period to positive correlation in future projections for eastern China.

1 Introduction

Global-scale warming has been unequivocal over the past century, and the global mean surface temperature is projected to increase by 1.4 to 4.8 °C by 2100 depending on different scenarios of greenhouse gas emissions (IPCC 2023). Within an anthropogenically warming climate, extreme weather and climate events have been shown to occur more frequently and intensely (Coumou and Rahmstorf 2012; Dosio et al.

2018). Many previous studies suggest increasing trends in extreme temperature, flood, and tropical cyclones over the past several decades, profoundly impacting the global ecosystem and socio-economic sectors (Hansen et al. 2012; Perkins et al. 2012; Westra et al. 2013; Fischer and Knutti 2015; Donat et al. 2016; Madakumbura et al. 2021; Thackeray et al. 2022).

HWs and EPEs are among the most threatening acute meteorological events, which have received considerable attention from policymakers, researchers, and the public (Stott et al. 2004; Lau and Nath 2012; Campbell et al. 2018; Li et al. 2018; Ning et al. 2022). Climate model projections have shown an increasing frequency of EPEs and HWs globally as the Earth's climate becomes warmer (O'Gorman and Schneider 2009; Fischer et al. 2013; Bao et al. 2017; Raghavendra et al. 2019; Li et al. 2019a). In addition to the changes in atmospheric circulation, extreme precipitation is more likely to occur in warmer seasons, because the saturation water vapor pressure increases by roughly 7%/°C according to the Clausius–Clapeyron relation (Boer 1993; Trenberth et al. 2003). Allan and Soden (2008) addressed the changes in extreme precipitation in a warmed climate and concluded that wet regions become wetter and dry regions become drier. However, the relationship between HWs and EPEs within the context of global warming (Cloutier-Bisbee et al. 2019), especially in the future, has not been fully studied.

China has experienced an increase in the frequency of HWs and EPEs during the past several decades (Sun and Ao 2013; Ma et al. 2015; Luo and Lau 2017; Ma et al. 2017; Zheng and Wang 2019) as well as compound heatwaves and heavy-precipitation events (Kong et al. 2020; Chen et al. 2021; Li et al. 2021; Ning et al. 2022). In 2022, China issued the first national red alert for extreme drought and heatwaves, with the maximum 2-m air temperature above 40 °C (104 °F) over 48 h or more in eastern China (defined as east of 100°E). Eastern China accounts for over 70% of the national population, highlighting its critical role in China's economic development (Zhu et al. 2011; Zhang et al. 2015). Thus, eastern China is vulnerable to summer HWs and EPEs (Sun et al. 2014; Chen et al. 2017; Zhang et al. 2017; Zhang and Zhou 2020). Population exposure to extreme drought is projected to increase by ~17% in China when the global temperature rises to 2 °C (Chen and Sun 2019). The frequent occurrence of HWs and EPEs in eastern China inevitably raises questions about changes in population exposure under current and future climates. Although the future population exposure of China under EPEs and HWs has been studied separately (Huang et al. 2018b; H. Chen et al. 2020; Chen and Sun 2021; Sun et al. 2021; Tang and Hu 2022; Wang et al. 2022), to the best of our knowledge, a comparative analysis of both has not been sufficiently implemented.

Global climate models are primary tools for investigating possible future changes in climate extremes (Jiang et al. 2015; Wang et al. 2019; Li et al. 2019b; Zhang et al. 2022). The Coupled Model Intercomparison Project Phase 6 (CMIP6) incorporates the most complete scientific experiments and the most simulation data of the past 20 years (Eyring et al. 2016; Simpkins 2017). Nevertheless, the commonality and difference between summer HWs and EPEs in the present and future have not yet been fully addressed by using the latest CMIP6 model ensemble.

In this study, we focused on examining the spatiotemporal variation characteristics and projections of HWs and EPEs in eastern China during extended summer (June–September) based on historical data (1979–2019) and CMIP6 models (2021–2100). The potential impacts of HWs and EPEs on population exposure in eastern China are evaluated from the present climate to future projections. Finally, we investigated the

connections between summer HWs and EPEs from the historical period to future different warming scenarios. Scientific answers to these questions are critical for understanding future vulnerability and developing mitigation and adaptation strategies.

2 Materials and methods

2.1 Study area

Eastern China (herein, defined as east of 100°E), adjacent to the Northwest Pacific Ocean and located in the East Asian summer monsoon region, has been widely considered in climate change studies (Dai et al. 2013; Sun et al. 2014). The Kuroshio Current, the subtropical western boundary current of the Northwest Pacific, plays a vital role in meridional heat transports, ocean-atmosphere interactions, and teleconnection (Pan et al. 2018; Chen et al. 2019). Eastern China is the most populous and economically developed region in China, with large urban aggregations. Hence,
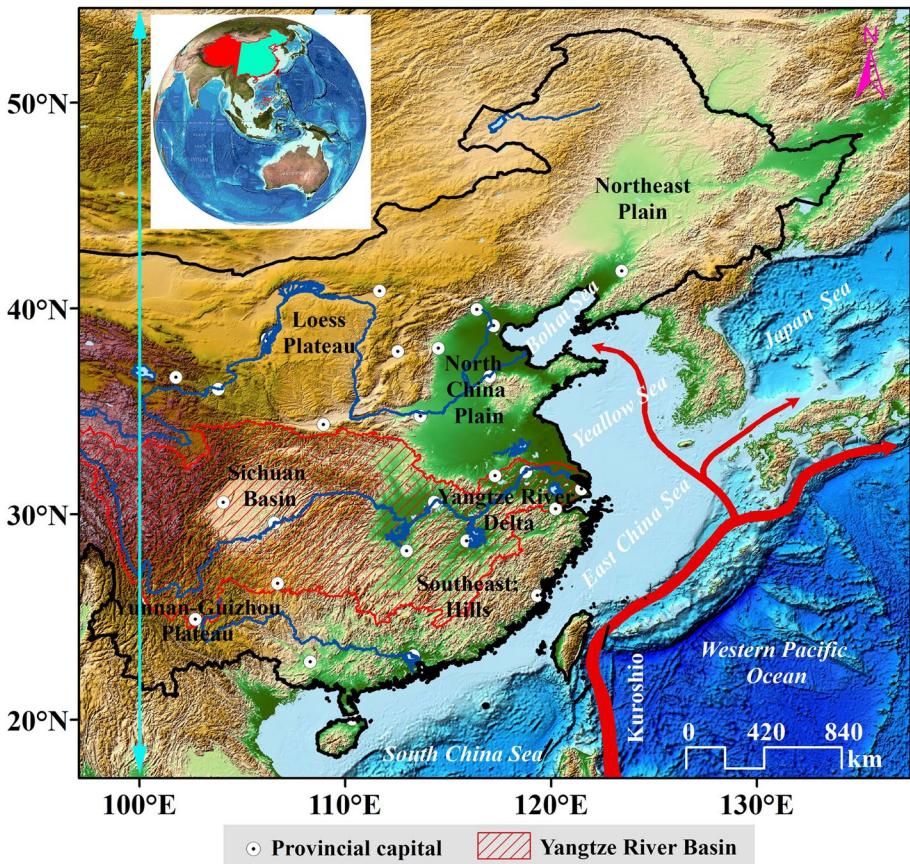

Fig. 1 Topography and the Kuroshio path in the study area. Eastern China is to the east of the cyan line (100 °E)

extreme weather and climate events profoundly impact people's daily lives in this specific region (Fig. 1).

2.2 Data sources

2.2.1 Observational data

The observational and reanalysis data used in this study are summarized in Table S1. The daily 2-m maximum surface air temperature (tasmax) and precipitation (pr) were obtained from the China Daily Surface Temperature/Precipitation Dataset (V2.0) at China Meteorological Data Service Center (CMDSC) based on 2472 meteorological stations in China (Chen et al. 2017). The data cover the period from January 1979 to December 2019.

The historical population density data in China were obtained from the Data Center for Resources and Environmental Sciences, Chinese Academy of Sciences (RESDC). This dataset includes historical population density every 5 years from 1990 to 2019 on 1-km grids (Xu 2017). The downscaled annual population data in China under different Shared Socioeconomic Pathways (SSPs) scenarios (1 km from 2010 to 2100) were applied following Y. Chen et al. (2020).

2.2.2 Future data preparation and model evaluation

The last version of the NASA Earth Exchange Global Daily Downscaled Projections (NEX-GDDP-CMIP6) dataset contains downscaled historical and future climate scenarios during 1950–2100 based on CMIP6 outputs. This dataset provides a set of global, bias-corrected (bias correction/spatial disaggregation method), high-resolution ($0.25° \times 0.25°$), and seamless climate variables (Thrasher et al. 2022). The daily tasmax and pr outputs from 24 models (Table S2) are used to assess the projected HWs and EPEs during 2021–2100. Here, we use only the models with outputs of the three simulations: historical, SSP245, and SSP585. SSP245 is considered a "middle of the road" pathway, which combines intermediate population growth, emission, and challenges, for both mitigation and adaptation, stabilizing at 4.5 W/m^2. On the other hand, SSP585 describes a "fossil-fueled development" pathway, incorporating rapid population growth and high emission, stabilizing at 8.5 W/m^2 and resulting in high challenges for mitigation (Costa and Rodrigues 2021). The multi-model ensemble mean method with equal weights is used to reduce model uncertainty. Furthermore, to be consistent with the length of the historical period (41 years), we divided the future period 2021–2100 into two subperiods: 2021–2060 and 2061–2100.

To evaluate the agreement of the daily historical tasmax and pr from CMIP6 with observations during the historical period 1979–2014, we use the Taylor diagrams to present the goodness of fit to observations by their correlation, centered root-mean-square difference (RMSD), and standard deviation (Taylor 2001). Fig. S1 displays the relative skills of tasmax and pr for 24 climate models in the extended summer (June–September). The performance of tasmax has a higher correlation and smaller RMSD and standard deviation than pr when comparing climate model outputs with observed data over the period with observations (1979–2014). However, the inter-model differences were relatively small for both variables, confirming the importance of the bias-adjusted CMIP6 products for the evaluation of regional extreme events. Therefore, we have retained all 24 models for analysis.

2.3 Methods

2.3.1 Definition of heatwaves

To better quantify the differences in regional climatology, a relative threshold (i.e., defined by percentile) for HWs is adopted in this study. Generally, the threshold for HW is mostly taken as 90th or 95th, which ensures that enough extreme events are detected each year and makes the analysis more statistically significant. For each calendar day, an HW event is identified if tasmax exceeded the 95th percentile threshold for at least three consecutive days based on the 1979–2019 climatology period (Hobday et al. 2016; Chen et al. 2017; Freychet et al. 2017). The climatological threshold is calculated from data within an 11-day window centered on each calendar day and then applied with a 31-day moving average. This seasonally varying threshold allows heatwave events to occur at any time of the year (Hobday et al. 2016). To calculate HWs in the future projections, we combine the period of 1979–2014 from the historical simulations and the period of 2015–2019 from the future projections as the baseline climatology thresholds, which is consistent with the observation. Following several previous studies (Wang et al. 2017; Yao and Wang 2021), we applied four metrics to represent annual HW characteristics, including the number of heatwaves per year (HWN), the total number of heatwave days per year (HWT), annual average duration within all heatwaves (HWDU), and annual average of maximum temperature above the baseline magnitude within all heatwaves (HWI). The details of their definition are listed in Table S3.

2.3.2 Extreme precipitation event

A threshold of 1 mm is typically used to distinguish between wet and dry days because extremely light precipitation (< 1 mm) may be occasionally recorded as no precipitation (Guo et al. 2018; Wu et al. 2018). Similarly, to represent the regional characteristics of precipitation changes, the relative threshold definition (the percentile-based method) is used to identify EPEs in this study (Huang et al. 2018a; Wu et al. 2018). Following Gao et al. (2017) and Huang et al. (2018a), we applied the 95th percentile to identify extremely high precipitation events in this study. Therefore, for each grid point in eastern China, an EPE was defined as the daily precipitation exceeding the 41-year average of the 95th percentile for the summers from 1979 to 2019. The method for calculating the 95th percentile precipitation is an empirical plotting position formula, which is simple and avoids any assumptions about the underlying distribution (Bonsal et al. 2001). For example, daily precipitation in summer (June to September) is first ranked in ascending order X_1, X_2, …, X_N. The probability P that a random value is less than or equal to the rank of that value X_m is estimated by

$$P = (m - 0.31)/(N + 0.38)$$

In the formula, m is the ordinal number of X_m, N is the length of the precipitation sequence (excluding days with precipitation less than 1 mm), and the 95th percentile value is the value of X_m corresponding to P=95%.

To calculate EPEs in the future projections, we combine the period of 1979–2014 from the historical simulations and the period of 2015–2019 from the future projections, which is consistent with the observation. If the precipitation at each grid cell exceeds this

threshold, an EPE is considered to have occurred. Furthermore, if an extreme precipitation event lasts for only 1 day, then it is termed as a 1-day EPE event. One-day EPE event is the major component of EPEs and can represent its main characteristics.

2.3.3 Calculation of population exposure

To evaluate the potential impacts of HWs (EPEs), we estimated the population exposure in eastern China by multiplying the population in each grid cell by the number of days of HWs (EPEs) for each corresponding grid cell over the specified period (Chen and Sun 2021). To match the climate data, the resolution of the population datasets was upscaled from 1 km to 0.25° using a summation method, and then the population exposure of the grid was calculated based on the 0.25° grid cells. In addition, Pearson's correlation analysis, linear trend analysis, and the Mann-Kendall test were conducted to calculate the correlation and trend of the HW or EPE metrics and their corresponding confidence levels (Hussain and Mahmud 2019).

3 Results

3.1 Spatiotemporal characteristics of summer EPEs during 1979–2019

As shown in Fig. 2, large spatial variations exist in the multi-year mean summer (June to September) frequency of EPEs and the amount of extreme precipitation (AEP) from 1979 to 2019. The regions with the highest EPEs appear in the south of the Yangtze River Basin and its western part, with an average of 3–5 EPEs year^{-1} in the past 41 summers (Fig. 2a). Meanwhile, the regions with high multi-year mean AEP appear in the eastern part of the study area and southeast coast, ranging from 60 to 112 mm (Fig. 2b). Notably, there is a spatial mismatch between multi-year means of EPEs and AEP, i.e., the high occurrence of EPEs is in the western, southern, and northeastern regions of the study area, whereas the high values of AEP are in the eastern part of the study area (Fig. 2a, b).

Moreover, the spatial pattern of the multi-year mean 1-day EPEs suggests consistency with a mean frequency of EPEs, with high values located in the south of the Yangtze River Basin and its western part, ranging from 3 to 5 counts (Fig. 2c). Meanwhile, the trend in annual mean 1-day EPEs is increased by 0.04 ± 0.02 ($p < 0.1$) counts per decade with significant interannual variation over 1979–2019 (Fig. 2d). The high-value area of annual mean total 1-day AEP is in the Yangtze River Basin and its southern coastal zone, ranging from 196 to 378 mm (Fig. 2e). In addition, the annual mean 1-day AEP shows an increasing trend during 1979–2019, reaching 3.23 ± 1.14 mm per decade ($p < 0.01$; Fig. 2f). In general, 1-day EPEs in eastern China have increased slowly over the past 40 years, but total 1-day AEP has increased significantly, suggesting that precipitation at individual EPE is increasing.

3.2 Spatiotemporal characteristics of summer HWs during 1979–2019

The high-value HWT areas are detected over the Yangtze River Basin and Loess Plateau, especially in the Yangtze River Delta and Sichuan Basin, where the corresponding HW duration ranges from 8 to 13 days (Fig. 3a). The high-value HWDU areas are relatively scattered, but they appear mainly in and around the Yangtze River Basin, and the
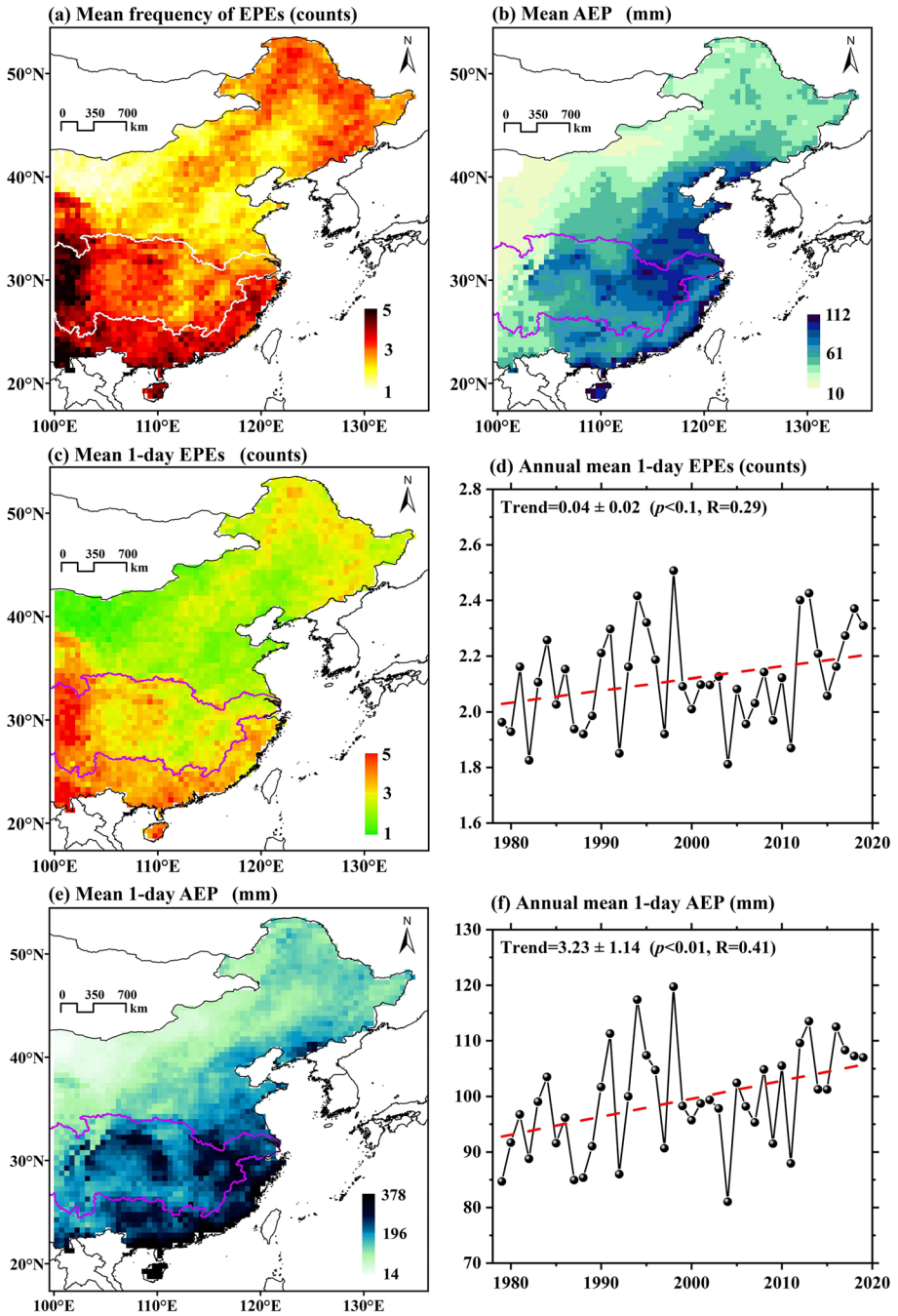
Fig. 2 Spatial distributions of the multi-year average summer **a** frequency of extreme precipitation events (EPEs), **b** amount of extreme precipitation (AEP), **c** 1-day EPEs, and **e** total 1-day AEP over 1979–2019. Time series of annual mean (area-weighted) summer **d** 1-day EPEs and **f** total 1-day AEP over 1979–2019. White and purple lines represent the Yangtze River Basin, and the dashed line represents the linear trend

Fig. 3 Spatial distributions of the multi-year means of summer heatwave metrics (left column) and their ▶ corresponding area-weighted temporal variations (right column) in eastern China from 1979 to 2019. **a**, **e** Mean HWT; **b**, **f** mean HWDU; **c**, **g** mean HWN; and **d**, **h** mean HWI. The blue lines delimit the Yangtze River Basin, and the dashed lines represent the linear trend

corresponding HW duration is 5–7 days/count (Fig. 3b). The HWN spatial pattern is consistent with that of HWT, but the high values also appear in the Northeast Plain (Fig. 3c). The HWI spatial pattern shows an increasing trend from south to north, reaching a maximum of 7–10 °C/count in northeastern China (Fig. 3d). Notably, high-value HWT and HWDU regions are both found in the Yangtze River Delta, which is the area with the most developed economy and densest population in China.

Additionally, increasing trends (± standard error) are observed in the regional averaged HW metrics (Fig. 3). Both HWT and HWN metrics exhibit rapid increases over 1979–2019, reaching 0.34±0.18 days per decade and 0.09 ± 0.03 counts per decade, respectively (Fig. 3e, g; $p < 0.01$). The trends in HWDU and HWI are 0.17 ± 0.07 days/count per decade and 0.11 ± 0.05 °C/count per decade over 1979–2019, respectively (Fig. 3f, h; $p < 0.1$). We note that the spatial patterns and temporal variations of both HWT and HWN are very similar. Since HWT is equal to HWN multiplied by HWDU, HWT is mainly affected by HWN (Fig. 3). Furthermore, summer HWs in eastern China have strong interannual variations, and severe HWs usually occur in major El Niño years (e.g., 1982/83, 1997/98, 2009/10).

3.3 HWs and EPEs in CMIP6 projection

Based on the CMIP6 model projections, we evaluate the spatiotemporal distribution of HWs and EPEs over 2021–2100 under two SSP scenarios. From 2021 to 2060, the values of HWT and HWDU in eastern China range from 12–36 days and 4–10 days/count under SSP245 scenario, respectively; the values of frequency of EPEs and AEP are 2–6 counts and 20–40 mm under SSP245 scenario, respectively (Fig. S2). In addition, there is no significant change in the above metrics from the SSP245 scenario to the SSP585 scenario. From 2061 to 2100, the values of HWT and frequency of EPEs reached 24–60 days and 4–6 counts under the SSP245 scenario, respectively; under the SSP585 scenario, the values reached 60–118 days and 5–8 counts, respectively (Fig. 4a, b). The coastal regions show relatively larger values of HWT and AEP than other regions in eastern China. HWT (AEP) reached 24–48 days (30–35 mm) under the SSP245 scenario and 60–108 days (35–40 mm) under the SSP585 scenario (Fig. 4c, d), suggesting that areas with high population densities in the coastal zone, which are vulnerable to HWs and EPEs, are expected to be more severely impacted. The regions with high HWDU and EPE frequencies are identified in the Yangtze River Basin and southern coastal regions under SSP585 scenario, reaching 10–50 days/count and 5–9 counts, respectively (Fig. 4f). In the southeast coast and southwest region of the study area, both HWDU and AEP show relatively high values, reaching 10–50 days/count and 25–35 mm under SSP585 scenario (Fig. 4h). While there is an increase in the values of HWN from SSP245 to SSP585 scenarios, it differs from HWT and HWDU in that there is less spatial variation between the two scenarios over the same future period (Figs. 3a, b; S4a, b). As for HWI, the differences in values and spatial variations are small for both scenarios and both future periods (Figs. S3c, d; S4c, d).

In future projections, the fast-growing HWT almost overlaps with areas where HWDU becomes longer. Specifically, the high values of multi-year mean HWT range from 8 to 13
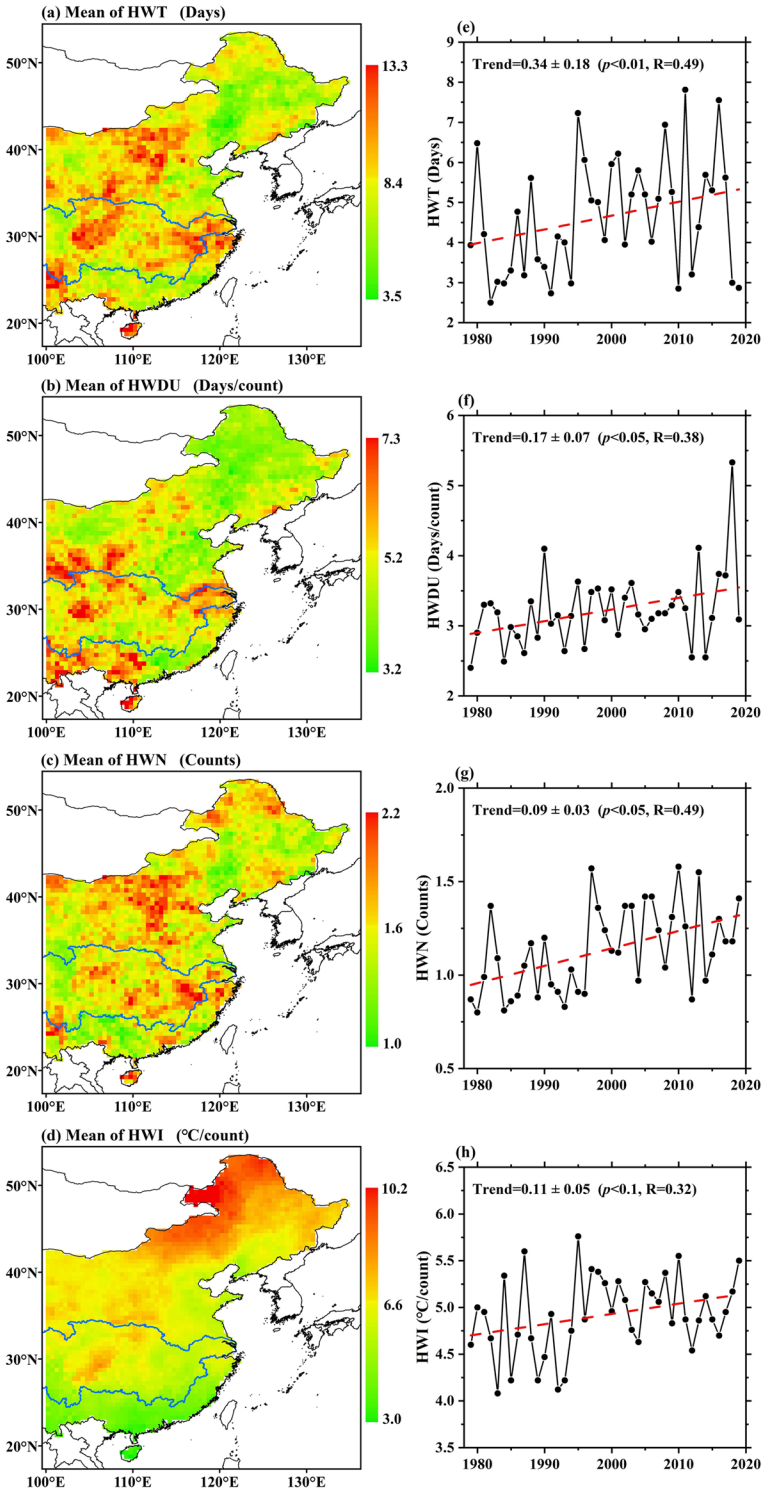
Fig. 4 Spatial distributions of multi-year averaged (left column) HWT (shaded area; unit: days) with the ▶ frequency of EPEs (blue contour line; unit: counts) and AEP (cyan contour line; unit: mm); (right column) HWDU (shaded area; unit: days/count) with the frequency of EPEs (blue contour line; unit: counts) and AEP (cyan contour line; unit: mm) under SSP245 (**a**, **c**, **e**, and **g**) and SSP585 (**b**, **d**, **f**, and **h**) scenarios in eastern China over 2061–2100. The purple lines present the Yangtze River Basin

days over 1979–2019 (Fig. 3), which are projected to increase to 24–60 days and 60–118 days under the SSP245 and SSP585 scenarios over 2061–2100 (Fig. 4). Meanwhile, the high values of multi-year mean EPEs and AEP extend from the southern coast to the Yangtze River Basin under the SSP585 scenario (Fig. 4). Thus, summer HWs and EPEs pose a dual threat to the future socioeconomic development of the Yangtze River Basin and its southern region.

### 3.4 Historical and future population exposure estimates

Population exposure describes the potential socioeconomic impacts of extreme events in a specific region. Consistent spatial patterns are detected for EPEs and HWs in eastern China during 1979–2019, with high population exposure in high-density population areas, such as the North China Plain, Yangtze River Delta, Sichuan Basin, and southeast coast (Fig. 5a, b). Time series of the annual mean population exposure affected by summer EPEs and HWs exhibit significantly rising trends, showing a growth rate of 15.7 ± 1.97 million person-days per decade for EPEs ($p < 0.01$) and 90.1 ± 14.1 million person-days per decade for HW ($p < 0.01$) (Fig. 5c, d). The population exposure to HWs is higher than that affected by EPEs in eastern China, and the increased rate of population exposure to HWs is nearly 6-fold than that of EPEs.

The total population exposure to EPEs shows a decreasing trend, from nearly 420 million person-days in the 2020s to 200 million person-days under the SSP245 scenario and 100 million person-days under the SSP585 scenario at the end of the twenty-first century (Fig. 6). The total population exposure to HWT under the SSP245 scenario shows a slower increasing trend, peaking at around 2096, reaching 3 billion person-days. Compared with the SSP245 scenario, we find a rapid increase in population exposure under the SSP585 scenario, which peaks around the 2080s (~5 billion person-days) and then stabilizes (Fig. 6). Considering the accelerated decrease in the total projected population in eastern China after 2040, the population exposures to EPEs and HWs show opposite trends. The population exposure to EPEs is decreasing rapidly in line with the population trend; however, the population exposure to HWs increases significantly, especially under the SSP585 scenario.

4 Discussion

4.1 Increased HWs and EPEs in a warming climate

Eastern China has experienced frequent HWs in recent decades, and such HWs are expected to increase in frequency, severity, and duration (Guo et al. 2017; Wang et al. 2017; Dosio et al. 2018; Li et al. 2019a; Ning et al. 2022). However, comparative differences in future HW and EPE changes in eastern China and background statistics are less known. For instance, the HWN is expected to increase rapidly under both the SSP245 and SSP585
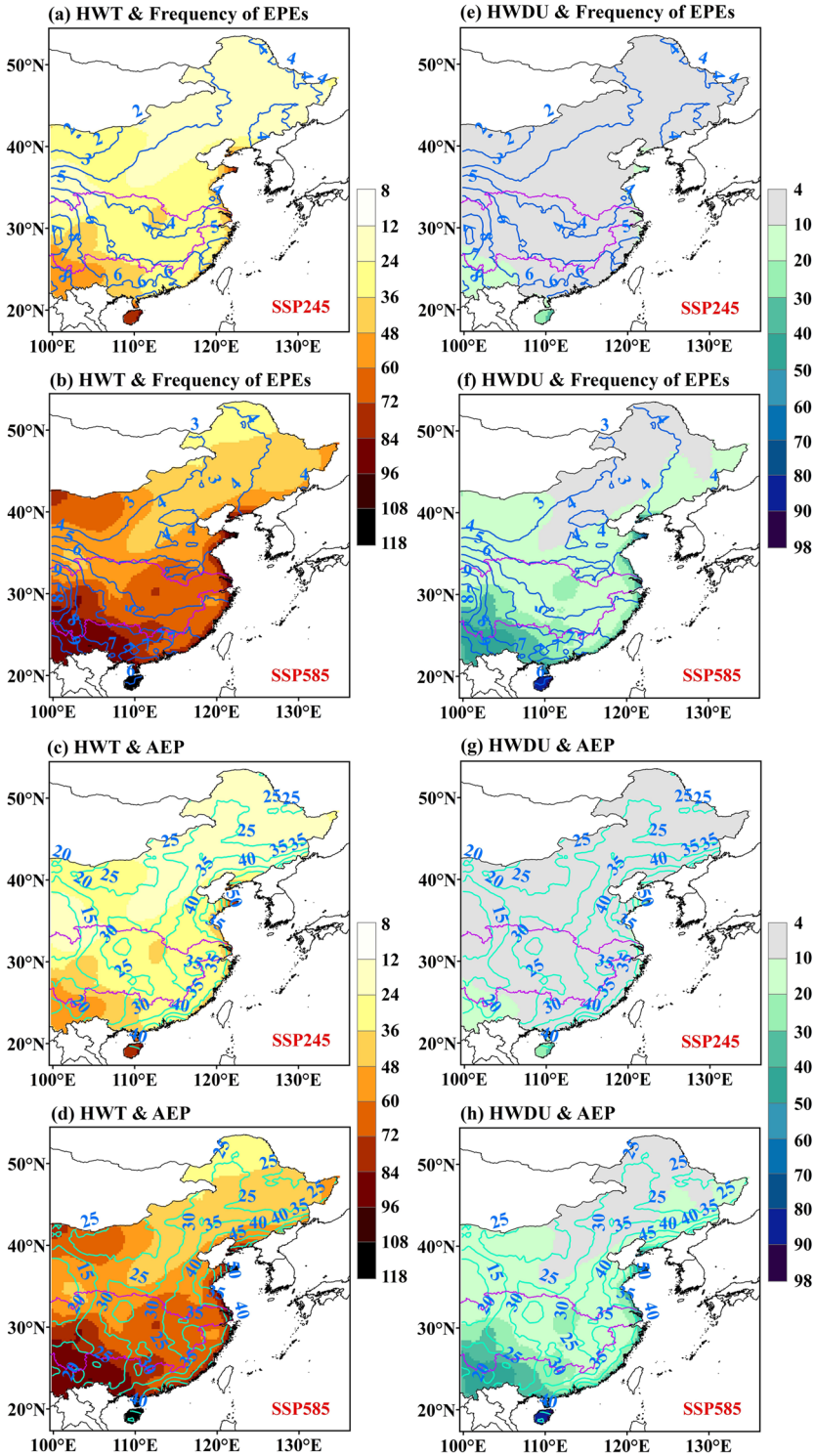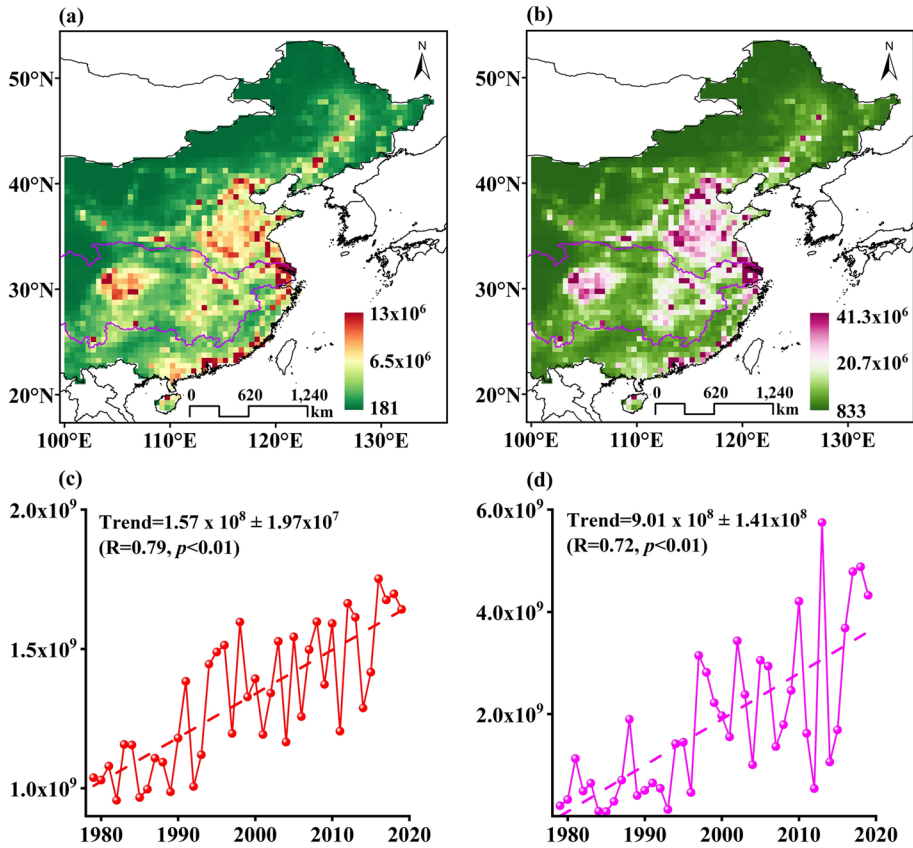
Fig. 5 Spatial patterns of multi-year mean population exposure affected by frequencies of **a** EPEs and **b** HWT in eastern China over 1979–2019 (unit: person-day). Time series of the annual total population exposure affected by summer **c** EPEs and **d** HWT over 1979–2019 (unit: person-day). Dashed lines represent the linear trend, and the purple lines represent the Yangtze River Basin

scenarios, and the trend of the frequency of EPEs under the SSP585 scenario is 2.0-fold than that under the SSP245 scenario (Fig. 7a, c). The number of EPEs has increased in eastern China and is projected to continue to rise through 2100, which is consistent with previous findings (Wang and Zhou 2005; Feng et al. 2011; Liu et al. 2015; Zhang et al. 2017; Dong et al. 2020). The increase in the atmospheric water-holding capacity associated with a temperature increase (the Clausius–Clapeyron relation) considerably influences the changes in extreme precipitation intensity at a rate of ~7%/°C under warmer climates (Pall et al. 2007; Allan and Soden 2008; Utsumi et al. 2011). Notably, the trends of HWT and AEP under the SSP585 scenario are 2.8-fold and 2.7-fold higher than those under the SSP245 scenario in the period 2021–2100, respectively (Fig. 7b, d).

The HWs are becoming more frequent, longer lasting, and more intense in eastern China under the global warming background (Figs. 3, 7). Notably, the longer HWDU leads to a rapid increase of HWT under the SSP585 scenario and thus a continued increase in the population exposure to HWs, though the future population in eastern China is projected to decrease (Figs. 6, S5). On the other hand, global warming will alter atmospheric circulation
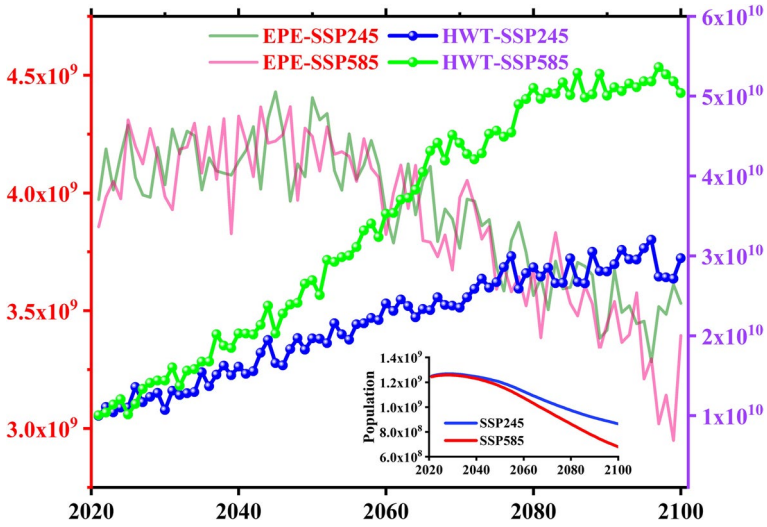
Fig. 6 Time series of annual total population exposure affected by summer EPE and HWT under SSP245 and SSP585 scenarios over 2021–2100 (unit: person-day). The inset chart represents the annual total population in eastern China under two future projections over 2021–2100. The left Y-axis scale (red) belongs to EPE, and the right Y-axis scale (purple) belongs to HWT
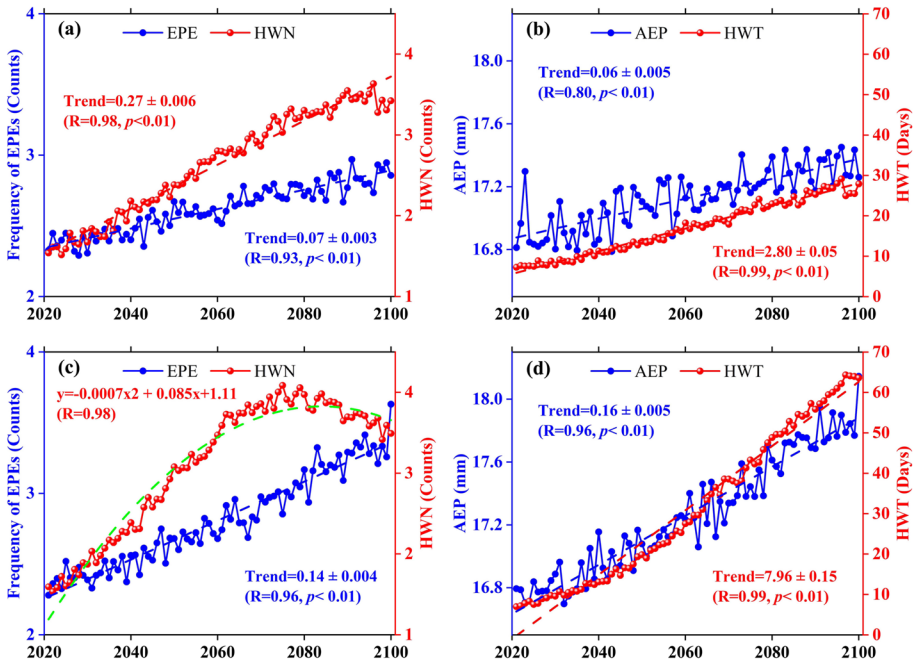

Fig. 7 Temporal variations of the annual averaged (area-weighted) summer frequency of EPEs and AEP compared with HWN and HWT under the SSP245 and SSP585 scenarios in eastern China over 2021–2100. **a** Frequency of EPEs and HWN under the SSP245 scenario, **b** AEP and HWT under the SSP245 scenario, **c** EPEs and HWN under the SSP585 scenario, and **d** AEP and HWT under the SSP585 scenario. Dashed blue and red lines represent the linear trends. The dashed green line represents the quadratic fit

Fig. 8 The correlation maps between annual mean summer **a**, **c**, and **e** precipitation and tasmax; **b**, **d**, and ▶
f frequencies of EPEs and HWs from the historical period (1979–2019) to future projections (2061–2100).
The areas significant at the 95% confidence level are dotted. The purple lines delimit the Yangtze River
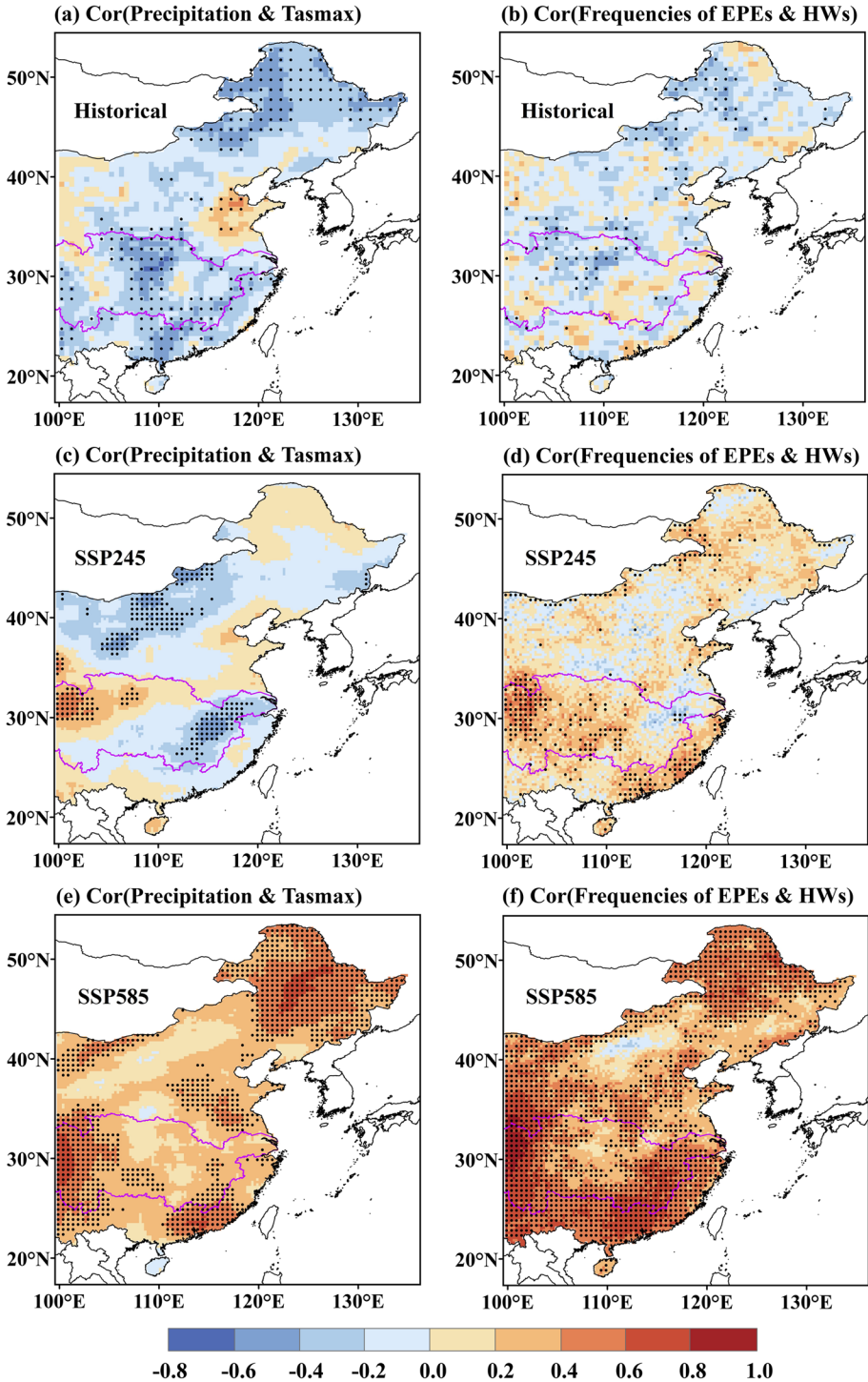Basin

and evaporation in some regions, providing a richer source of water for precipitation (IPCC
2018). Global warming and the resulting changes in atmospheric circulation increase the
probability of EPEs in humid regions (Allan and Soden 2008). Both the rapidly increasing
EPEs and AEP indicate that the Yangtze River Basin and the southeast coast will remain
key areas affected by extreme precipitation in the future (Figs. S6, 7). Overall, the Yangtze
River Basin and the southern coast are projected to face a compound hazard of HWs and
EPEs in summer as a hotspot for regional climate change in the future.

4.2 Relationship between HWs and EPEs from present climate to future projections

Anthropogenic factors (e.g., greenhouse gas emissions and land-use change) contribute
to the rising occurrence of heavy precipitation and high-temperature extremes globally
(Fischer and Knutti 2015; Dosio et al. 2018). The rapid increase in the risk of summer
HWs and EPEs in eastern China can also be partially attributed to global warming (Sun
et al. 2014; Liu et al. 2015; Freychet et al. 2017; Guo et al. 2023). For tasmax in eastern
China, under the SSP245 and SSP585 scenarios, the warming amplitude at the end of
the twenty-first century relative to the pre-industrial period is close to 5 °C and 8 °C,
respectively (Fig. S8). Sea surface temperature anomalies also play an important role
in modulating HWs and EPEs in China (Zhu et al. 2011; Wang et al. 2017; Wei et al.
2020). Furthermore, summer EPEs and HWs in eastern China are closely related to the
strength and location of the western North Pacific subtropical high (Zhu et al. 2011;
Freychet et al. 2017; Zhang et al. 2017).

  EPEs and HWs are influenced by various factors, yet their evolving relationship
under global warming remains crucial. Intuitively, we expect cooler summers when it
rains, while heatwaves often accompany droughts (Trenberth and Shea 2005). During
1979–2019, the correlation between annual mean precipitation and tasmax is negative
in almost all eastern China (−0.8–0.4), whereas it shifts to positive in some areas of
eastern China under the SSP245 scenario over 2061–2100 (0.2–0.6; $p < 0.05$), and then
extends to almost the entire eastern China under the SSP585 scenario over 2061–2100
(0.2–1.0; $p < 0.05$) (Fig. 8a, c, e). Climate models suggest that EPEs and HWs will
become more common in an anthropogenically warm climate (IPCC 2023). The corre-
lations between the frequencies of EPEs and HWs also shift from negative in the histor-
ical period (1979–2019) to positive under future projections (Fig. 8b, d, f). The above
phenomenon is also present in the future period 2021–2060 (Fig. S9). These results
reveal a distinct link between future rainfall and temperature, with increased EPEs sig-
nificantly associated with HWs during summer (Raghavendra et al. 2019). In addition,
summer precipitation and maximum temperature were negatively correlated during
1979–2019, consistent with the argument that warmer summers tend to be dryer, but
this negative correlation is reduced in extreme cases.

  HWs are strongly linked to global warming, and previous studies have shown a signif-
icant increase in global HW activity from present climate to future projections (Hu et al.
2003; Freychet et al. 2017; Dosio et al. 2018; Perkins-Kirkpatrick and Lewis 2020). In
addition, the compound disasters of HWs and EPEs are becoming more frequent under

(a) Cor(Precipitation & Tasmax)

(b) Cor(Frequencies of EPEs & HWs)

(c) Cor(Precipitation & Tasmax)

(d) Cor(Frequencies of EPEs & HWs)

(e) Cor(Precipitation & Tasmax)

(f) Cor(Frequencies of EPEs & HWs)

global warming (Kong et al. 2020; Chen et al. 2021; Li et al. 2021; Ning et al. 2022). In eastern China, as the correlations between the frequencies of EPEs and HWs shift from negative to positive in the future throughout the entire future period (2021–2100) (Fig. S10), this could lead to loss of lives and property and enormous socioeconomic consequences in the future. This further underscores the urgent need for policymakers to act decisively in reducing greenhouse emissions and achieving the goal of net-zero carbon emission.

5 Conclusions

EPEs and HWs contribute significantly to socioeconomic losses and human health risks, particularly in the densely populated and economically vibrant regions of eastern China. This study investigated the current and future spatiotemporal characteristics of EPEs and HWs in eastern China and their impacts on population exposure in a warming world. The main conclusions are as follows:

1. The regions with the largest EPEs are apparent in the western part of the Yangtze River Basin and its southern area, with an average of 3–5 EPEs year^{-1} during 1979–2019; the regions with large mean AEP appear in the eastern part of the study area and southeast coast, ranging from 60 to 112 mm. Various metrics of HW show increasing trends over 1979–2019, and the increased HWN resulted in a rapid increase of HWT, with rates of 0.09 ± 0.03 counts per decade and 0.34 ± 0.18 days per decade, respectively.
2. In terms of future spatial variation, high values of multi-year mean HWT are 24–60 days and 60–118 days under the SSP245 and SSP585 scenarios during 2061–2100, respectively. The longer HWDU leads to a rapid increase in HWT. The high values of multi-year mean EPEs and AEP extend from the southern coast to the Yangtze River Basin under the SSP585 scenario during 2061–2100. In terms of temporal variation, HWs and EPEs are both increasing in future projections. According to multi-model projections, the Yangtze River Basin and its southern region will face the increase of compound disasters due to the occurrence of summer HWs and EPEs.
3. In the period from 1979 to 2019, the North China Plain, Yangtze River Delta, Sichuan Basin, and southeast coast are the areas with high multi-year mean total population exposure under the influence of EPEs and HWs. The annual mean total population exposure to EPEs and HWs shows increasing trends during 1979–2019, with the latter increasing 5.7-fold faster than the former. In future projections, the annual mean total population exposure to EPEs decreases from 0.4 billion to 0.3 billion person-days, while the population exposure to HWs shows an increasing trend, reaching peak values of over 3 billion and 5 billion person-days under SSP245 and SSP585 scenarios, respectively.
4. By the end of the twenty-first century, the warming amplitude of tasmax in eastern China relative to the pre-industrial period is close to 5 °C and 8 °C under the SSP245 and SSP585 scenarios, respectively. We detected a strong positive correlation between mean-state (tasmax and pr) and extreme climate (HWs and EPEs) in future projections. In eastern China, summer precipitation and maximum temperature were negatively correlated, consistent with the argument that warmer summers tend to be dryer. As the correlations between the frequencies of EPEs and HWs shift from negative to positive

in the future, this could lead to loss of lives and property and enormous socioeconomic consequences in the future.

Finally, there are some unavoidable uncertainties in the projection of future changes in extreme events. Taylor diagram shows that the correlation coefficient of summer precipitation in eastern China ranges from 0.6 to 0.8, which is lower than that of maximum temperature (Fig. S1). In addition, multi-model ensemble mean precipitation overestimates EPEs and underestimates AEP when compared to observations from 1979 to 2019 (Figs. S6, 7). Therefore, more observations to downscale and bias correct the raw CMIP6 model outputs would be beneficial for regional studies (Meng et al. 2022; Guo et al. 2023). Human-caused climate change was the main driver of the weather and climate extremes, such as heatwaves and heavy precipitation (IPCC 2023). Although we revealed that the relationship between EPEs and HWs shifts from negative in the present climate to positive in future projections, the physical mechanism behind this phenomenon needs further investigation. We assume that increases in HWT from the historical period to future projections may compress the precipitation time window, leading to an increase in EPEs and AEP.

Declarations

Conflict of interest The authors declare no competing interests.

References

Allan RP, Soden BJ (2008) Atmospheric warming and the amplification of precipitation extremes. Science 321:1481–1484

Bao J, Sherwood SC, Alexander LV et al (2017) Future increases in extreme precipitation exceed observed scaling rates. Nat Clim Chang 7:128–132

Boer G (1993) Climate change and the regulation of the surface moisture and energy budgets. Clim Dyn 8:225–239

Bonsal BR, Zhang X, Vincent LA et al (2001) Characteristics of daily and extreme temperatures over Canada. J Clim 14:1959–1976

Campbell S, Remenyi TA, White CJ et al (2018) Heatwave and health impact research: a global review. Health Place 53:210–218

Chen H, Sun J (2019) Increased population exposure to extreme droughts in China due to 0.5 °C of additional warming. Environ Res Lett *14*:064011

Chen H, Sun J (2021) Significant increase of the global population exposure to increased precipitation extremes in the future. *Earths*. Future 9(9):e2020EF001941

Chen Y, Hu Q, Yang Y et al (2017) Anomaly based analysis of extreme heat waves in Eastern China during 1981–2013. Int J Climatol 37:509–523

Chen C, Wang G, Xie S et al (2019) Why does global warming weaken the Gulf Stream but intensify the Kuroshio? J Clim 32:7437–7451

Chen Y, Guo F, Wang J et al (2020) Provincial and gridded population projection for China under shared socioeconomic pathways from 2010 to 2100. Sci Data 7:83

Chen Y, Liao Z, Shi Y et al (2021) Detectable increases in sequential flood-heatwave events across China during 1961-2018. Geophy Res Lett *48*(6):e2021GL092549

Cloutier-Bisbee SR, Raghavendra A, Milrad SM (2019) Heat waves in Florida: climatology, trends, and related precipitation events. J Appl Meteor Climatol 58:447–466

Costa NV, Rodrigues RR (2021) Future summer marine heatwaves in the western south Atlantic. Geophys Res Lett 48:e2021GL094509

Coumou D, Rahmstorf S (2012) A decade of weather extremes. Nat Clim Chang 2:491–496

Dai A, Li H, Sun Y et al (2013) The relative roles of upper and lower tropospheric thermal contrasts and tropical influences in driving Asian summer monsoons. J Geophys Res: Atmos 118:7024–7045

Donat MG, Lowry AL, Alexander LV et al (2016) More extreme precipitation in the world's dry and wet regions. Nat Clim Chang 6:508–513

Dong G, Jiang Z, Tian Z et al (2020) Projecting changes in mean and extreme precipitation over eastern China during 2041–2060. Earth Space Sci 7:e2019EA001024

Dosio A, Mentaschi L, Fischer EM et al (2018) Extreme heat waves under 1.5 °C and 2 °C global warming. Environ Res Lett 13:054006

Eyring V, Bony S, Meehl G et al (2016) Overview of the Coupled Model Intercomparison Project Phase 6 (CMIP6) experimental design and organization. Geosci Model Dev 9:1937–1958

Feng L, Zhou T, Wu B et al (2011) Projection of future precipitation change over China with a high-resolution global atmospheric model. Adv Atmos Sci 28:464–476

Fischer EM, Knutti R (2015) Anthropogenic contribution to global occurrence of heavy-precipitation and high-temperature extremes. Nat Clim Chang 5:560–564

Fischer EM, Beyerle U, Knutti R (2013) Robust spatially aggregated projections of climate extremes. Nat Clim Chang 3:1033–1038

Freychet N, Tett S, Wang J et al (2017) Summer heat waves over Eastern China: dynamical processes and trend attribution. Environ Res Lett 12:024015

Gao T, Wang H, Zhou T (2017) Changes of extreme precipitation and nonlinear influence of climate variables over monsoon region in China. Atmos Res 197:379–389

Guo X, Huang J, Luo Y et al (2017) Projection of heat waves over China for eight different global warming targets using 12 CMIP5 models. Theor appl climat 128:507–522

Guo X, Wu Z, He H et al (2018) Variations in the start, end, and length of extreme precipitation period across China. Int J Climatol 38:2423–2434

Guo J, Wang X, Fan Y et al (2023) How extreme events in China would be affected by global warming-insights from a bias-corrected CMIP6 ensemble. Earth's. Future 11:e2022EF003347

Hansen J, Sato M, Ruedy R (2012) Perception of climate change. P Nat Acad Sci 109:E2415–E2423

Hobday AJ, Alexander LV, Perkins SE et al (2016) A hierarchical approach to defining marine heatwaves. Prog Oceanogr 141:227–238

Hu Z, Yang S, Wu R (2003) Long-term climate variations in China and global warming signals. J Geophys Res: Atmos 108:4614

Huang W, He X, Yang Z et al (2018a) Moisture sources for wintertime extreme precipitation events over south China during 1979–2013. J Geophys Res: Atmos 123:6690–6712

Huang D, Zhang L, Gao G (2018b) Projected changes in population exposure to extreme heat in China under a RCP8.5 scenario. J Geograph Sci 28(10):1371–1384

Hussain M, Mahmud I (2019) pyMannKendall: a python package for non parametric Mann Kendall family of trend tests. J Open Source Software 4(39):1556

IPCC (2018) Global warming of 1.5 °C. Cambridge University Press, Cambridge, UK and New York, NY, USA, pp 3–24

IPCC (2023) Climate change 2023: synthesis report. In: Contribution of working groups I, II and III to the sixth assessment report of the Intergovernmental Panel on Climate Change. IPCC, Geneva, Switzerland, pp 1–34

Jiang Z, Li W, Xu J et al (2015) Extreme precipitation indices over China in CMIP5 models. Part I: Model evaluation J Clim 28:8603–8619

Kong Q, Guerreiro SB, Blenkinsop S et al (2020) Increases in summertime concurrent drought and heat-wave in Eastern China. Weather Clim Extremes *28*:100242

Lau NC, Nath MJ (2012) A model study of heat waves over North America: meteorological aspects and projections for the twenty-first century. J Clim 25:4761–4784

Li W, Jiang Z, Zhang X et al (2018) Additional risk in extreme precipitation in China from 1.5 °C to 2.0 °C global warming levels. Sci Bull 63:228–234

Li Z, Guo X, Yang Y et al (2019a) Heatwave trends and the population exposure over China in the 21st century as well as under 1.5° C and 2.0° C global warmer future scenarios. Sustainability 11:3318

Li Y, Ren G, Wang Q et al (2019b) More extreme marine heatwaves in the China Seas during the global warming hiatus. Environ Res Lett 14:104010

Li K, Wang M, Liu K (2021) The study on compound drought and heatwave events in China using complex networks. Sustainability 13(22):12774

Liu R, Liu S, Cicerone RJ et al (2015) Trends of extreme precipitation in eastern China and their possible causes. Adv Atmos Sci 32:1027–1037

Luo M, Lau NC (2017) Heat waves in southern China: synoptic behavior, long-term change, and urbanization effects. J Clim 30:703–720

Ma S, Zhou T, Dai A et al (2015) Observed changes in the distributions of daily precipitation frequency and amount over China from 1960 to 2013. J Clim 28:6960–6978

Ma S, Zhou T, Stone DA et al (2017) Attribution of the July–August 2013 heat event in central and eastern China to anthropogenic greenhouse gas emissions. Environ Res Lett 12:054020

Madakumbura GD, Thackeray CW, Norris J et al (2021) Anthropogenic influence on extreme precipitation over global land area seen in multiple observational datasets. Nat Commun 12:3944

Meng Y, Hao Z, Feng S et al (2022) Multivariate bias corrections of CMIP6 model simulations of compound dry and hot events across China. Environ Res Lett 17:104005

Ning G, Luo M, Zhang W et al (2022) Rising risks of compound extreme heat-precipitation events in China. Int J Climatol 42:5785–5795

O'Gorman PA, Schneider T (2009) The physical basis for increases in precipitation extremes in simulations of 21st-century climate change. P Nat Acad Sci 106:14773–14777

Pall P, Allen M, Stone DA (2007) Testing the Clausius–Clapeyron constraint on changes in extreme precipitation under CO2 warming. Clim Dyn 28:351–363

Pan J, Feng X, Lai W et al (2018) Barrier effects of the Kuroshio current on the East Asian northerly monsoon: a sensitivity analysis. Sci Rep 8:18044

Perkins S, Alexander L, Nairn J (2012) Increasing frequency, intensity and duration of observed global heat-waves and warm spells. Geophys Res Lett 39:L20714

Perkins-Kirkpatrick S, Lewis SC (2020) Increasing trends in regional heatwaves. Nat Commun 11:3357

Raghavendra A, Dai A, Milrad SM et al (2019) Floridian heatwaves and extreme precipitation: future climate projections. Clim Dyn 52:495–508

Simpkins G (2017) Progress in climate modelling. Nat Clim Chang 7:684–685

Stott PA, Stone DA, Allen MR (2004) Human contribution to the European heatwave of 2003. Nature 432:610–614

Sun J, Ao J (2013) Changes in precipitation and extreme precipitation in a warming environment in China. Chinese Sci Bull 58:1395–1401

Sun Y, Zhang X, Zwiers FW et al (2014) Rapid increase in the risk of extreme summer heat in Eastern China. Nat Clim Chang 4:1082–1085

Sun S, Dai T, Wang Z et al (2021) Projected increases in population exposure of daily climate extremes in eastern China by 2050. Adv Clim Change Res 12(6):804–813

Tang B, Hu W (2022) Significant increase in population exposure to extreme precipitation in South China and Indochina in the future. Sustainability *14*(10):5784

Taylor KE (2001) Summarizing multiple aspects of model performance in a single diagram. J Geophys Res: Atmos 106:7183–7192

Thackeray CW, Hall A, Norris J et al (2022) Constraining the increased frequency of global precipitation extremes under warming. Nat Clim Chang 12:441–448

Thrasher B, Wang W, Michaelis A et al (2022) NASA global daily downscaled projections, CMIP6. Sci Data 9(1):262

Trenberth KE, Shea DJ (2005) Relationships between precipitation and surface temperature. Geophys Res Lett 32:L14703

Trenberth KE, Dai A, Rasmussen RM et al (2003) The changing character of precipitation. Bull Am Meteorol Soc 84:1205–1218

Utsumi N, Seto S, Kanae S (2011) Does higher surface temperature intensify extreme precipitation? Geophys Res Lett 38:L16708

Wang Y, Zhou L (2005) Observed trends in extreme precipitation events in China during 1961–2001 and the associated changes in large-scale circulation. Geophys Res Lett 32:L09707

Wang P, Tang J, Sun X et al (2017) Heat waves in China: definitions, leading patterns, and connections to large-scale atmospheric circulation and SSTs. J Geophys Res: Atmos 112:10679–10699

Wang P, Hui P, Xue D et al (2019) Future projection of heat waves over China under global warming within the CORDEX-EA-II project. Clim Dyn 53:957–973

Wang L, Rohli RV, Lin Q et al (2022) Impact of extreme heatwaves on population exposure in China due to additional warming. Sustainability *14*(18):11458

Wei J, Wang W, Shao Q et al (2020) Heat wave variations across China tied to global SST modes. J Geophys Res: Atmos 125:e2019JD031612

Westra S, Alexander LV, Zwiers FW (2013) Global increasing trends in annual maximum daily precipitation. J Clim 26:3904–3918

Wu X, Guo S, Yin J et al (2018) On the event-based extreme precipitation across China: time distribution patterns, trends, and return levels. J Hydrol 562:305–317

Xu X (2017) The 1 km grid dataset of China's population spatial distribution. https://www.resdc.cn/DOI/DOI.aspx?DOIid=32.

Yao Y, Wang C (2021) Variations in summer marine heatwaves in the south China sea. J Geophys Res: Oceans 126:e2021JC017792

Zhang W, Zhou T (2020) Increasing impacts from extreme precipitation on population over China with global warming. Sci Bull 65:243–252

Zhang W, Pan S, Cao L et al (2015) Changes in extreme climate events in eastern China during 1960–2013: a case study of the Huaihe River Basin. Quatern Int 380:22–34

Zhang Q, Zheng Y, Singh VP et al (2017) Summer extreme precipitation in eastern China: mechanisms and impacts. J Geophys Res: Atmos 122:2766–2778

Zhang W, Kirtman B, Siqueira L et al (2022) Decadal variability of southeast US rainfall in an eddying global coupled model. Geophys Res Lett 49:e2021GL096709

Zheng J, Wang C (2019) Hot summers in the Northern Hemisphere. Geophys Res Lett 46:10891–10900

Zhu Y, Wang H, Zhou W et al (2011) Recent changes in the summer precipitation pattern in East China and the background circulation. Clim Dyn 36:1463–1473

Authors and Affiliations

Yulong Yao[1,2] · Wei Zhang[3,4] ⓘ · Ben Kirtman[5]

✉   Wei Zhang
     dr.weizhang@outlook.com

[1]   State Key Laboratory of Tropical Oceanography, South China Sea Institute of Oceanology, Chinese Academy of Sciences, Guangzhou, China

[2]   Global Ocean and Climate Research Center, South China Sea Institute of Oceanology, Chinese Academy of Sciences, Guangzhou, China

[3]   Program in Atmospheric and Oceanic Sciences, Princeton University, Princeton, NJ 08540-6654, USA

[4]   National Oceanic and Atmospheric Administration/Global Systems Laboratory, Boulder, CO 80305, USA

[5]   Rosenstiel School of Marine and Atmospheric Science, University of Miami, Miami, FL, USA